

17 **Abstract**

18 In underwater diving, decompression schedules are based on compartmental models of
19 nitrogen and helium tissue kinetics. However these models are not based on direct
20 measurements of nitrogen and helium kinetics. In isoflurane anesthetized sheep,
21 nitrogen and helium kinetics in the hind limb (n=5) and brain (n=5) were determined
22 during helium-oxygen breathing and after return to nitrogen-oxygen breathing.
23 Nitrogen and helium concentrations in arterial, femoral vein, and sagittal sinus blood
24 samples were determined using headspace gas chromatography and venous blood flows
25 were monitored continuously using ultrasonic Doppler. The experiment was repeated at
26 different states of hind limb blood flow and cerebral blood flow. Using arterial blood
27 gas concentrations and blood flows as input, parameters and model selection criteria of
28 various compartmental models of hind limb and brain were estimated by fitting to the
29 observed venous gas concentrations. In both the hind limb and brain, nitrogen and
30 helium kinetics were best fit by models with multi-exponential kinetics. In the brain,
31 there were no differences in nitrogen and helium kinetics. Hind limb models fit to the
32 two gases separately indicated nitrogen kinetics were slightly faster than helium, but
33 models with the same kinetics for both gases fit the data well. In the hind limb and
34 brain, the blood:tissue exchange of nitrogen is similar to that of helium. Based on these
35 results, it is inappropriate to assign substantially different time constants for nitrogen
36 and helium in all compartments in decompression algorithms.

37

Keywords:

Gases
Pharmacokinetics
Decompression Sickness

38

39 Glossary

B1	fractional size of compartment 1
c_1	compartment 1 helium or nitrogen concentration (mL mL^{-1})
c_2	compartment 2 helium or nitrogen concentration (mL mL^{-1})
c_{art}	arterial helium or nitrogen concentration (mL mL^{-1})
$c_{\text{pre-cap}}$	pre-capillary (end-arterial) helium or nitrogen concentration (mL mL^{-1})
$c_{\text{end-cap}}$	end-capillary helium or nitrogen concentration = c_1 (mL mL^{-1})
c_{ven}	sagittal sinus or femoral vein helium or nitrogen concentration (mL mL^{-1})
F1	fraction of blood flow directed to first compartment
PS	permeability \times surface area coefficient between compartment 1 and 2 (mL min^{-1})
PSC	permeability \times surface area coefficient between arterial and venous blood (mL min^{-1})
Q	blood flow (mL min^{-1})
V_1	compartment 1 apparent volume (mL)
V_2	compartment 2 apparent volume (mL)
V_{tot}	total apparent volume = $V_1 + V_2$ (mL)
V_{ven}	countercurrent venous blood volume (mL)

40 Introduction

41 Compartmental models of blood:tissue exchange of inert gases are used to describe the
42 pharmacokinetics of anesthetic gases, calculate tissue blood flow, and to manage the
43 risk of decompression sickness. A compartment is a tissue volume represented by a
44 single, time-varying chemical activity. This 'well-mixed' representation assumes that,
45 owing to rapid diffusion, equilibration of inert gas chemical activity gradients across
46 the tissue region represented by the compartment is much faster than transport in and
47 out of the compartment. The most simple and commonly used tissue model is the
48 single, well-mixed compartment in which perfusion is often considered the rate limiting
49 process. In this model, arterial-tissue inert gas chemical activity difference declines
50 mono-exponentially and can be characterized by a single time constant.

51 Tissue kinetics of inert gases are often better described by multiple exponentials. Multi-
52 exponential kinetics can be accommodated by models with multiple compartments.
53 Multi-exponential kinetics are often attributed to heterogeneous tissue perfusion and
54 represented by a collection of perfusion-limited compartments with different time
55 constants (20). However, multi-exponential kinetics may arise because of diffusion-
56 limited exchange of gas between tissue regions (5,24,26,29). Such diffusion
57 phenomena can be described with multiple compartments separated by diffusion
58 permeable membranes (11,12).

59 Blood:tissue exchange has been examined for a variety inert of gases (which we define
60 as gases that are nonionizable and are not metabolized). Hydrogen, xenon, krypton, and
61 nitrous oxide have received the most attention (2,5,9,13,20,23) because they are used as
62 tracers for calculation of blood flow using the indirect Fick method (10,19). Nitrogen

63 and helium are of interest for two reasons. Firstly, nitrogen and helium differ in
64 diffusivities and solubilities from each other and from other gases which have been
65 studied, and the relative importance of perfusion and diffusion may be determined by
66 examining the kinetics of tracers with differing physicochemical properties. Secondly,
67 nitrogen and helium are components of breathing mixtures for deep sea diving.
68 Decompression sickness occurs in compressed gas underwater diving, as well as in
69 space flight and aviation, as a result of intracorporeal bubble formation from excess
70 dissolved gas upon reduction in ambient pressure (decompression). The risk of
71 decompression sickness is managed using decompression schedules calculated using
72 compartmental models of the kinetics of nitrogen and helium in tissues. In
73 decompression models, time constants for nitrogen and helium in any compartment are
74 often presumed to differ substantially, but these time constants are not based on direct
75 measurement of nitrogen and helium kinetics.

76 There are very few data examining the tissue kinetics of nitrogen and none where the
77 tissue nitrogen is mass-balanced and suitable for fit of kinetic models (1,8). We have
78 previously reported mass-balanced, kinetic data for helium in cerebral and skeletal
79 muscle tissue, and evaluated competing compartmental models based on their fit to the
80 data collected from individual animals (11,12). At the time of collecting these helium
81 data, we simultaneously measured the kinetics of nitrogen in some animals; however,
82 owing to contamination of some samples with atmospheric nitrogen, the remaining
83 nitrogen data from individual animals was sparse, and not suitable for evaluating
84 models. In this report, we fit conventional perfusion-limited models and diffusion-
85 limited models previously found to best fit individual animal data, to mean data across

86 all animals to explore for any major differences in the isobaric exchange of nitrogen
87 and helium.

88 Methods

89 **Ethical Approval**

90 All surgical and experimental procedures were approved by the University of Adelaide
91 and Institute of Medical and Veterinary Sciences animal ethics committees and were
92 conducted in accordance with the *Australian Code of Practice for the Care and Use of*
93 *Animals for Scientific Purposes* (National Health and Medical Research Council. 1997.
94 6th ed. Australian Government Publishing Service, Canberra).

95 **Initial surgical preparation and brain study design**

96 Eight healthy adult Merino ewes weighing approximately 50 kg were anesthetized and
97 instrumented as previously described (30,31). Two 7-French gauge catheters were
98 positioned in the thoracic aorta via the right femoral artery for measurement of blood
99 pressure and for arterial blood sampling. We have previously shown that the arterial
100 helium concentration-time curves determined simultaneously from aorta and more
101 peripheral arterial sampling sites are indistinguishable at the precision of the present
102 assay (12). A multi-lumen pulmonary artery floatation catheter was introduced via the
103 right jugular vein and used in these experiments for intravenous drug administration
104 and monitoring core temperature. Via a craniotomy a 20 MHz ultrasonic Doppler flow
105 probe (Titronics Medical Instruments, IA, U.S.A.) was placed on the sagittal sinus for
106 measurement of an index global cerebral blood flow and a 4-French catheter placed in
107 the sagittal sinus for sampling of effluent blood from the cerebral hemispheres. The
108 craniotomy was sealed with dental acrylic. On recovery from anesthesia the sheep were
109 housed in metabolic crates with free access to food and water for at least two days
110 recovery from surgery and between experimental days.

111 Five of the eight sheep were used in the brain studies. On the experimental day, sheep
112 were anesthetized with 250 mg i.v. propofol (David Bull Laboratories, NSW, Australia)
113 induction, 1.5% isoflurane (Abbott Australia, NSW, Australia) maintenance and
114 mechanically ventilated via an endotracheal tube. Sheep were placed on their side. The
115 closed circuit anesthetic system was supplied with a fresh gas flow of 5 L min^{-1} of 22%
116 oxygen monitored at the common gas outlet (Capnomac, Datex, Helsinki, Finland) and
117 the balance nitrogen. Ultrasonic Doppler frequency shifts from the sagittal sinus probe
118 were measured using a pulsed Doppler flow meter (Bioengineering, University of Iowa,
119 Iowa City, IA, USA). Mean arterial blood pressure was measured using a transducer on
120 the arterial catheter. Doppler and pressure signals were digitized at 1 Hz (DAS 16-G2,
121 Metrabyte, MA, USA) and recorded continuously to a micro-computer. End tidal
122 carbon dioxide partial pressure was monitored (Cardiicap, Datex, Helsinki, Finland) on
123 the outlet of the endotracheal tube.

124 After a minimum of 45 minutes for the induction agent to be cleared from the blood,
125 physiological measurements were made during a period of normocarbica and then either
126 a low or a high cerebral blood flow state (randomized order) was produced by either
127 hyperventilating the sheep and reducing the end tidal carbon dioxide to about 20 mmHg
128 or hypoventilating and increasing the end tidal carbon dioxide to about 50 mmHg,
129 respectively. When the physiological measurements were stable, steady state values
130 were recorded during a five minute baseline period then nitrogen was replaced by
131 helium in the anesthetic circuit fresh gas flow (no net change in oxygen or total gas
132 flow) for 15 min.

133 Paired arterial and sagittal sinus blood samples for nitrogen and helium analysis were
134 taken during the baseline period and then at 1, 2, 3, 4, 6, 8, 11, 15, 16, 17, 18, 19, 21,
135 23, 26, 30, and 35 minutes from the beginning of helium breathing. Additional arterial
136 samples only were taken at 0.5 and 15.5 minutes. For each sample, after withdrawal of
137 5 mL blood to remove catheter dead space, approximately 3 mL blood was drawn over
138 10 to 15 s with a fresh 3 mL syringe and immediately injected via a 26 gauge needle
139 through the butyl rubber septum of a sealed, weighed, argon-filled glass headspace vial
140 of precisely 22 mL volume. Dead space blood was replaced and the catheter flushed
141 with 5 mL of heparinized 0.9% saline. To minimize sample contamination with
142 environmental gas “Safti-ject” SV valves (Codan US Corp., CA, USA) that have no
143 luer hub dead space were used on the catheters and the hubs of the syringes and 26
144 gauge needles were filled with heparinized saline. To exclude atmospheric nitrogen, the
145 sampling apparatus was sealed inside a clear plastic bag accessed via latex wrist seals
146 and continuously flushed with argon.

147 Sixty minutes after helium administration the alternative cerebral blood flow state was
148 produced and once end tidal carbon dioxide and cerebral blood flow were stable at the
149 new level, the helium administration and blood sampling described above was repeated.

150 **Hind limb surgical preparation and study design**

151 Five of the eight sheep (two of which had been used in the brain study) were used in
152 the hind limb studies. On the experimental day, sheep were anesthetized, mechanically
153 ventilated, and monitored in the same manner as in the brain study. Sheep were placed
154 on their back and the left femoral artery and vein were exposed. A cuffed ultrasonic
155 Doppler flow probe was mounted around the left femoral vein. Doppler frequency shift
156 provides an index of femoral vein blood flow and was recorded at a sampling rate of 1

157 Hz using a four-channel pulsed Doppler flow meter, digitized, and recorded
158 continuously to microcomputer. A 4-French blood sampling catheter was introduced
159 into the left femoral vein 2.5 cm proximal to the Doppler probe and the tip advanced
160 towards the leg close to the probe. Heparin (25,000 i.u.) was then given intravenously
161 to prevent clots forming in the femoral vein that hindered blood sampling. Cotton tape
162 was tied around the tarsal region of the left leg to reduce contamination of femoral
163 venous blood with blood from the hoof and shank. Validation of this hind limb blood
164 flow method in these sheep has been previously described and resulting femoral vein
165 blood is predominantly skeletal muscle effluent. (31).

166 Throughout the experimental day surgery and subsequent study the sheep were
167 mechanically ventilated via an endotracheal tube and the closed circuit anesthetic
168 system was supplied with a fresh gas flow of 5 L min^{-1} of 22% oxygen and the balance
169 nitrogen. End tidal carbon dioxide partial pressure was maintained between 37 to
170 42 mm Hg. Mean arterial pressure was maintained near 100 mm Hg using infusions of
171 0.9% saline as necessary. Room temperature was approximately 22°C . Body
172 temperature was maintained using an electrical heating pad beneath the sheep.

173 A minimum of two hours following induction of anesthesia, additional heparin (25,000
174 i.u.) was given intravenously and then stable, steady state values of physiological
175 measurements were recorded during a five minute baseline period. Then nitrogen was
176 replaced by helium in the anesthetic circuit fresh gas flow (no net change in oxygen or
177 total gas flow) for 20 min. Paired arterial and femoral vein blood samples for nitrogen
178 and helium analysis were taken during the baseline period and then at 1, 2, 3, 4, 6, 8,
179 11, 15, 20, 21, 22, 23, 24, 26, 28, 31, 35, 40, and 50 minutes from the beginning of

180 helium breathing. Blood samples were taken in the same manner as described for the
181 brain study.

182 Next, a 26 gauge needle was inserted into the left femoral artery and a low hind limb
183 blood flow state was produced by an infusion of epinephrine (Astra Pharmaceuticals,
184 NSW, Australia), diluted to 1 mg in 50 mL in saline and infused at 0.3 to 1 mL min⁻¹.
185 Once flow was stable at the new level for approximately 10 min, and a minimum of
186 70 min washout after the previous helium administration, the helium administration and
187 blood sampling described above was repeated. At the end of the study, the femoral vein
188 Doppler probe signal was calibrated against timed collections of femoral venous blood
189 outflow and blood flow in mL min⁻¹ calculated.

190 **Nitrogen and helium analysis**

191 Nitrogen and helium concentration in blood samples was analyzed using a headspace
192 gas chromatographic system comprising an 8500 series gas chromatograph with
193 thermal conductivity detector and an HS-101 series automated headspace sampler
194 (Perkin Elmer, Beaconsfield, UK) in-line between the carrier gas supply and column.
195 Argon carrier gas flow was 15 mL min⁻¹. Samples were passed through a 1 m long by
196 2 mm i.d. pre-column packed with 50% silica gel / 50% activated charcoal to absorb
197 water and CO₂, and sample gas separation was achieved on a 2 m long by 2 mm i.d.
198 stainless steel column packed with molecular sieve 5A 80/100 mesh. The reference
199 channel of the thermal conductivity detector was also supplied with argon at 15 mL
200 min⁻¹ via another molecular sieve 5A column. Column temperature was 75°C and
201 detector temperature was 80°C.

202 Sample volume was determined from sample weight (mg) assuming a blood specific
203 gravity of 1.03 g mL⁻¹. The headspace sample vials were left un-agitated at room
204 temperature for a minimum of one hour (generally three to eight hours) to allow
205 equilibration of the blood and headspace. We previously determined that blood and
206 headspace equilibrated in less than one hour by equilibrating blood with helium and
207 then injecting samples of this blood into argon-filled headspace vials as previously
208 described (12) and then analyzing these samples at different times after injecting the
209 blood. Vial headspace was pressurized with carrier gas (246 kPa) and sampled using a
210 timed (6 s) injection. Blood nitrogen and helium concentrations, expressed as mL gas
211 per mL blood at room temperature and atmospheric pressure, was estimated by
212 comparison of blood sample headspace nitrogen and helium peak area with six point
213 standard curves produced by injecting argon-filled headspace vials with measured
214 volumes of helium or nitrogen (0 – 25 µL) using a gas tight syringe and analyzing these
215 standards in the identical manner as were the blood samples. The mean r^2 value for the
216 standard curves was 0.967 (S.D. = 0.028). Blood sample headspace nitrogen and helium
217 peak areas were adjusted for sample volume by multiplying by $\lambda_b + V_{HS}/V_b$ where V_{HS}
218 and V_b are the volumes of the vial headspace and blood sample and λ_b is the published
219 helium or nitrogen Ostwald blood solubility at room temperature (22). We previously
220 determined that λ_b for helium in sheep blood is similar to published values from other
221 species and any differences have negligible effect since V_{HS}/V_b is approximately 800
222 times larger than λ_b and nitrogen and helium partition predominantly into the
223 headspace. Assay sensitivity was approximately 10^{-4} mL gas per mL blood.

224 Data for individual animals was examined and data points were excluded by the
 225 following criteria: for both nitrogen and helium data, occasional assay failures resulted
 226 in unusually low values which were excluded; and nitrogen data points were excluded
 227 if considered to result from atmospheric contamination, for instance values higher than
 228 that corresponding to blood equilibrated with air. Figure 1 shows an example of the
 229 nitrogen and helium data from the individual animals and the forcing functions
 230 representing the mean arterial data and the mean venous values used for model fitting.

231 **Data analysis**

232 A collection of compartment models were used as structural models for inert gas
 233 kinetics in brain and hind limb tissue and were constructed as ordinary differential
 234 equations using the Scientist for Windows software package (Version 2.01, MicroMath
 235 Scientific Software, UT, USA). Diagrammatic representations of the models are given
 236 in Tables 2 and 3. The model equations are given below.

237 **Perfusion-diffusion model**

238
$$V_1 \frac{dc_{ven}}{dt} = Q(c_{art} - c_{ven}) + PS(c_2 - c_{ven}) \quad (1)$$

239
$$V_2 \frac{dc_2}{dt} = PS(c_{ven} - c_2) \quad (2)$$

240 **Perfusion-limited model**

241
$$V_1 \frac{dc_{ven}}{dt} = Q(c_{art} - c_{ven}) \quad (3)$$

242 **Perfusion-limited countercurrent diffusion model**

243
$$V_1 \frac{dc_1}{dt} = Q(c_{art} - c_{ven}) \quad (4)$$

244
$$V_{ven} \frac{dc_{ven}}{dt} = Q(c_1 - c_{ven}) + PSC(c_{art} - c_{ven}) \quad (5)$$

245

246 In the present models, since inert gases are freely diffusible, intravascular,
 247 extravascular, extracellular, and intracellular spaces could comprise a single

248 compartment. A unity partition coefficient between tissue and blood ($\lambda_t/\lambda_b = 1$, where
249 λ_t is the Ostwald tissue solubility) and between compartments 1 and 2 was assumed. In
250 the countercurrent diffusion models, diffusion of gas is assumed to occur between
251 precapillary vessels and postcapillary vessels that are parallel and have countercurrent
252 flow, such as may occur between centripetal arteries and centrifugal veins in the brain
253 or transverse arterioles and venules in skeletal muscle. As a simplifying assumption,
254 the change in inert gas concentration along any element of the arterial vessel is
255 accompanied by an equivalent change along the corresponding element of the venous
256 vessel, so that there is a constant arterial-venous nitrogen and helium concentration
257 difference across the countercurrent exchange region and $c_{\text{art}} - c_{\text{ven}} = c_{\text{pre-cap}} - c_{\text{end-cap}}$. This
258 model of countercurrent exchange is illustrated in figure 1 of reference (25). Additional
259 general assumptions were that the system was linear and total tissue volume (V_{tot}) was
260 stationary between blood flow states.

261 Model inputs for each flow state were time-varying forcing functions (sums of
262 exponentials) representing the mean arterial blood nitrogen and helium concentrations
263 (c_{art}) (see Figure 1) and mean values of hind limb and cerebral blood flow. Although
264 the uncalibrated Doppler signal is sufficient for model input, to provide more
265 meaningful model parameter estimates, flow in mL min^{-1} (Q) were estimated from
266 Doppler signal. The mean hind limb blood flow, calculated from the calibrated Doppler
267 signal, in the low flow state was 14 mL min^{-1} and in the resting flow state was 63 mL
268 min^{-1} . The sagittal sinus Doppler signal was not directly calibrated in these sheep,
269 instead the Doppler signal during normocarbica was assumed to represent a flow of 34
270 mL min^{-1} as previously measured (30), and the low and high flows estimated from the
271 change in the Doppler signal with hypocarbica and hypercarbica. The resulting mean

272 cerebral blood flow used for model input in the low flow state was 20 mL min^{-1} and in
273 the high flow state was 63 mL min^{-1} . For comparison, cerebral blood flow was
274 previously calculated from the arterial and venous helium concentration curves using
275 the indirect Fick method assuming a unity partition coefficient between tissue and
276 blood (10,12). The resulting mean (S.D.) cerebral blood flow in these five sheep in the
277 low flow state was $24 (6) \text{ mL } 100 \text{ mL}^{-1} \text{ min}$ and in the high flow state was $98 (46) \text{ mL}$
278 $100 \text{ mL}^{-1} \text{ min}$, in close agreement with the sagittal sinus Doppler estimates considering
279 the sagittal sinus drains approximately 60-70 mL of brain tissue (17,30).

280 Models were solved numerically using variable step size Adams-Moulton and
281 Backwards Differentiation Formula methods of the EPISODE solver for stiff and non-
282 stiff systems (7). Parameters of each brain and hind limb model were estimated by
283 fitting the model simultaneously to the observed high and low flow mean venous blood
284 nitrogen and helium concentrations by least squares non-linear regression. Models were
285 fit to the mean helium data alone and to the mean nitrogen data alone to evaluate if
286 differences in kinetics between the two gases resulted in different parameter estimates.
287 Models were also fit simultaneously to the nitrogen and helium data with common
288 parameter estimates for the two gases, to examine the consequences of requiring
289 identical kinetics for the two gases. Thus the models were tested for their ability to
290 describe the change in kinetics of each gas resulting from altered flow states and for
291 their ability to describe kinetics of the different gases. Within each data set, models
292 were compared using a Model Selection Criterion (MSC), a modified Akaike
293 Information Criterion calculated in Scientist for Windows:

$$294 \quad \text{MSC} = \ln \left(\frac{\sum_{i=1}^n (Y_{obs_i} - \bar{Y}_{obs})^2}{\sum_{i=1}^n (Y_{obs_i} - Y_{cal_i})^2} \right) - \frac{2p}{n} \quad (6)$$

295 Where Y_{obs_i} , Y_{cal_i} , and \bar{Y}_{obs} are the observed values, the fitted values, and the mean of
 296 the observed data points respectively, n is the number of data points, and p is the
 297 number of parameters required to obtain the fit. A large MSC indicates good model fit
 298 to the data but the MSC is penalized for model complexity (number of estimated
 299 parameters, p).

300 Results

301 The parameter estimates and MSC for the various structural models of the brain fit to
302 the mean brain data are given in Table 1. The fit of the single perfusion-limited
303 compartment model to the mean sagittal sinus nitrogen and helium concentrations is
304 illustrated in Figure 2. This single-compartment model provides good fit to the high
305 cerebral blood flow data, but overestimates the uptake and washout of nitrogen and
306 helium in the low flow state. All models with multi-exponential kinetics provided
307 improved fit to the low blood flow data compared to the single-compartment model,
308 without compromising fit to the high blood flow data. There was little difference in the
309 MSC between the multi-exponential models, but for the combined nitrogen and helium
310 data, the perfusion-diffusion model of the brain achieved the highest MSC. The fit of
311 the perfusion-diffusion model to the mean sagittal sinus nitrogen and helium
312 concentrations is illustrated in Figure 3. This model, in which nitrogen and helium have
313 identical kinetics appears to fit these data well.

314 The parameter estimates and MSC for the various structural models of the hind limb fit
315 to the mean data are given in Table 2. A single perfusion-limited tissue compartment
316 model fit the hind limb data poorly (MSC 1.81 for fit to the combined nitrogen and
317 helium data) and is not given in Table 2, but the data are well described by two
318 exponentials. The countercurrent model of the hind limb achieved the best fit to the
319 nitrogen alone, helium alone, and the combined data sets. The fit of the countercurrent
320 model to the mean femoral vein nitrogen and helium is illustrated in Figure 4. This
321 model, in which nitrogen and helium have identical kinetics appears to fit these data
322 well.

323 Unlike what was found for the brain, structural models of the hind limb with common
324 estimates of permeability×surface area coefficient parameters (PS and PSC) across
325 flow states provided poor fit to the data (not shown), and the models in Table 2 have a
326 separate estimate of PS and PSC for each flow state.

327 For all the structural models of the brain and hind limb, similar parameter estimates
328 arose from fit to the mean helium data alone, fit to the mean nitrogen data alone, and
329 simultaneous fit to the nitrogen and helium data, with few exceptions. In fitting the
330 countercurrent diffusion model of the brain to the nitrogen data alone, the best MSC
331 was achieved with an estimate for PSC an order of magnitude higher than for fit to the
332 helium or the combined inert gases data. For all the structural models of the hind limb,
333 estimated apparent volumes from fit to the helium data alone were higher than for the
334 nitrogen data alone, suggesting that helium may equilibrate with the hind limb more
335 slowly than nitrogen. This difference may not be large since the models with a single
336 value for apparent volume provided good fit to the nitrogen and helium data. There was
337 no systematic variation in the estimated apparent volumes for the brain models,
338 indicating that nitrogen and helium exchange at similar rates in the brain.

339 Discussion

340 The ranking of the structural models based on the present fits to mean nitrogen and
341 helium data are consistent with previous results of model fits to helium data from
342 individual animals (11,12). The single perfusion-limited tissue compartment predicts
343 that the arterial-venous concentration difference declines mono-exponentially. Such a
344 model fit the high blood flow data for the brain, but this model does not fit the low
345 blood flow brain data or either flow state for the hind limb data. This adds to the
346 considerable body of evidence for multi-exponential kinetics of inert gases in brain and
347 skeletal muscle (2,11,12,20,23,28,29). Two parallel perfusion-limited compartments
348 with large differences in relative compartmental blood perfusion fit the data quite well.
349 However, the estimated differences in perfusion are larger than have been measured
350 between different tissue regions in the brain (17,21) or in the hind limb (4,18,23). The
351 perfusion-diffusion model and the countercurrent model provided the best fits to the
352 data. There was little difference in the fits of these two models to the data.

353 In the present study all models were lumped models, which assume well-mixed
354 compartments. The consequence of assuming instantaneous mixing of the gases in the
355 compartments can be examined by order of magnitude comparison of time constants for
356 compartment mixing by diffusion and flow into and out of the compartments.

357 Compartment mixing can be characterized by time constants for radial (perpendicular
358 to capillary) diffusion and axial (parallel to capillary) diffusion. Mixing to less than 1%
359 difference occurs, by definition, in 4.6 time constants ($\ln 100/\text{rate constant}$, where rate
360 constant = $1/\text{time constant}$). Of the two tissues investigated, skeletal muscle has the
361 larger inter-capillary distance ($2r$) = 0.005 cm (16,27), and unlike the brain, skeletal
362 muscle has a parallel arrangement of capillaries that can allow for axial concentration

363 gradients. Of the two gases, nitrogen has the lower diffusion coefficient
364 ($D = 1.3 \times 10^{-5} \text{ cm}^2 \text{ s}^{-1}$ (22)). Nitrogen exchange in the hind limb is therefore most likely
365 to depart from the well-mixed behavior. The time constant for radial diffusion of
366 nitrogen in skeletal muscle is $r^2/D = 0.48 \text{ s}$ and radial mixing time is
367 $\ln 100 \ r^2/D = 0.037 \text{ min}$. Skeletal muscle capillary tissue unit length (x) = 0.1 cm and
368 mean capillary blood velocity (v) = 0.05 cm s^{-1} (16,27). The time constant for axial
369 diffusion of nitrogen is $x^2/D = 769 \text{ s}$, and the time constant for capillary perfusion is
370 $x/v = 2 \text{ s}$. Axial mixing is dominated by the capillary perfusion and that mixing time is
371 $\ln 100 \ x/v = 0.15 \text{ min}$. Both radial and axial mixing times are an order or more of
372 magnitude smaller than the fastest time constant for flow into and out of any hind limb
373 model compartment: $V_{\text{ven}}/Q = 2.7 \text{ min}$ (countercurrent model, combined nitrogen and
374 helium hind limb parameter estimates, high blood flow state). Other hind limb time
375 constants are one to two orders of magnitude larger, indicating that consideration of
376 concentration gradients across capillary tissue units is not relevant to the time course of
377 the present studies and the well-mixed assumption is appropriate.

378 Fit of all the structural models of the hind limb to the nitrogen data alone resulted in
379 estimated compartment volumes about 25% smaller than those estimated by fit to the
380 helium data alone. This difference in compartment apparent volumes (V_1 , V_2 , V_{tot}) can
381 be partially accounted for by the use of a unity partition coefficient for both gases; the
382 apparent volume is equal to the true volume times the partition coefficient. Published
383 solubility coefficients for nitrogen and helium, all in species other than sheep (22),
384 indicate a helium partition coefficient between muscle and blood of about 1.18 and a
385 nitrogen partition coefficient between brain and blood of about 1.06. The difference
386 between these latter values and unity only accounts for about a 10% difference in hind

387 limb apparent volume estimates. It is possible the remaining difference in apparent
388 volumes for the two gases may be due to loss of helium from the system, but models
389 that include a term for loss of helium were not justified by the data (data not shown).
390 The remaining differences in estimated apparent volumes for the two gases indicates
391 slower kinetics of helium than nitrogen in the hind limb. Such a difference may not be
392 truly resolvable by fit of the structural models to the mean data. Indeed models with the
393 same volume estimates for the two gases, and therefore the same kinetics, fit the data
394 well.

395 These findings have implications for decompression algorithms. The majority of
396 decompression algorithms model the kinetics of inert gases in a collection of
397 compartments with different time constants spanning the range of tissues kinetics
398 relevant to decompression sickness. Decompression algorithms that accommodate
399 multiple gases may assign different time constants to nitrogen and helium for the same
400 compartment. This structure is appropriate for compartments with slow gas exchange,
401 as evidenced by slower whole-body washout of nitrogen than of helium (3,14). This
402 slower washout of nitrogen than helium from tissues with slow gas exchange probably
403 underlies the slower required decompression from nitrogen-oxygen than from helium-
404 oxygen saturation dives (15). Saturation dives are hyperbaric exposures of sufficient
405 duration that all body tissues have equilibrated with inspired inert gas partial pressure,
406 and the slowest washout of gas from tissues limits the rate of decompression from such
407 dives. However, some decompression algorithms assign faster time constants for
408 helium than for nitrogen in all compartments (6). The present findings indicate this
409 latter structure is not appropriate, since nitrogen and helium exchange at similar rates in
410 some tissues. For the best of the present models, the slowest compartment time constant

411 for a normal blood flow state was $V_1/Q = 24$ min (countercurrent model, combined
412 nitrogen and helium hind limb parameter estimates), which is relatively fast in terms of
413 the collection of time constants used in decompression algorithms. The extent of gas
414 uptake into compartments with fast time constants determines the deepest required
415 decompression stop for dives of insufficient duration for all body tissues to reach
416 equilibration with inspired inert gas partial pressure (bounce dives). A deeper first
417 decompression stop results in longer total decompression time. In models structures
418 with faster helium than nitrogen uptake into fast compartments, a deeper first
419 decompression stop and longer total decompression results from a helium-oxygen
420 bounce dive than from a nitrogen-oxygen bounce dive to the same depth for the same
421 bottom time. This behavior may be inappropriate, but there are few data directly
422 comparing the decompression obligation resulting for helium-oxygen and nitrogen-
423 oxygen bounce dives of identical depth and duration.

424 In summary, this is the first report of mass mass-balanced, kinetic data for isobaric
425 tissue exchange of nitrogen and helium. In both the brain and the hind limb, the
426 blood:tissue exchange of nitrogen is similar to that of helium. These kinetics are best
427 described by two exponential processes, possibly as a consequence of arterial-venous
428 shunt of these highly diffusible solutes.

429 **Acknowledgements**

430 Current address for D. J. Doolette: Navy Experimental Diving Unit, Panama City, USA

431 We thank A. Martinez for technical assistance.

432 The authors acknowledge that the Australian Centre for Pharmacometrics is an
433 initiative of the Australian Government as part of National Collaborative Research
434 Infrastructure Strategy.

435 **Grants**

436 This work was conducted in part while Dr Doolette was a Jean B. Reid Medical
437 Research Associate, Health Science Research Committee, the University of Adelaide.

438 Partially funded by a grant from the National Health and Medical Research Council of
439 Australia. Grant 970067: Pharmacokinetics of gases: Development of integrated
440 experimental and modeling methods.

441 Partially funded by a grant from the University of Adelaide – Division of Health
442 Sciences Research Committee. Grant: Pharmacokinetics of gases: Development of
443 integrated experimental and modeling methods.

444 **Disclosures**

445 The authors have no competing interest with respect to this manuscript

446

447 References

448

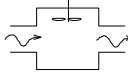
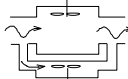
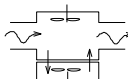
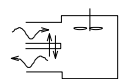
- 449 1. **Ackles, K. N., Holness, D. E., and Scott, C. A.** Measurement of uptake and
450 elimination of nitrogen in tissue, *in vivo*. In: *Underwater Physiology V*, edited
451 by Lambertsen CJ. Bethesda: FASEB, 1976.
- 452 2. **Aukland K, Akre S, and Leraand S.** Arteriovenous counter-current exchange of
453 hydrogen gas in skeletal muscle. *Scand J Clin Lab Invest Suppl 99*: 72-75,
454 1967.
- 455 3. **Behnke AR and Willmon TL.** Gaseous nitrogen and helium elimination from
456 the body during rest and exercise. *Am J Physiol* 131: 619-626, 1940.
- 457 4. **Bell AW, Hales JRS, King RB, and Fawcett AA.** Influence of heat stress on
458 exercise-induced changes in regional blood flow in sheep. *J Appl Physiol* 55:
459 1916-1923, 1983.
- 460 5. **Brodersen P, Sejrsen P, and Lassen NA.** Diffusion bypass of xenon in brain
461 circulation. *Circ Res* 32: 363-369, 1973.
- 462 6. **Bühlmann AA.** Experimentelle Grundlagen der risikoarmen Dekompression
463 nach Überdruckexpositionen. *Schweiz Med Wochenschr* 112: 48-59, 1982.
- 464 7. **Byrne GD, Hindmarsh AC, Jackson KR, and Brown HG.** A comparison of
465 two ODE codes: GEAR and EPISODE. *Comput Chem Eng* 1: 133-147, 1977.
- 466 8. **Campbell JA and Hill L.** Studies in the saturation of the tissues with gaseous
467 nitrogen.-I. Rate of saturation of goat's bone marrow *in vivo* with nitrogen
468 during exposure to increased atmospheric pressure. *Quart J Exp Biol* 23: 197-
469 210, 1933.
- 470 9. **Doolette DJ, Upton RN, and Grant C.** Diffusion limited, but not perfusion
471 limited, compartmental models describe cerebral nitrous oxide kinetics at both
472 high and low cerebral blood flows. *J Pharmacokinet Biopharm* 26: 649-672,
473 1998.
- 474 10. **Doolette DJ, Upton RN, and Grant C.** Agreement between ultrasonic Doppler
475 venous outflow and Kety-Schmidt estimates of cerebral blood flow. *Clin Exp*
476 *Pharmacol Physiol* 26: 736-740, 1999.
- 477 11. **Doolette DJ, Upton RN, and Grant C.** Countercurrent compartmental models
478 describe hind limb skeletal muscle helium kinetics at resting and low blood
479 flows in sheep. *Acta Physiol Scand* 185: 109-121, 2005.
- 480 12. **Doolette DJ, Upton RN, and Grant C.** Perfusion-diffusion compartmental
481 models describe cerebral helium kinetics at high and low cerebral blood flows
482 in sheep. *J Physiol (Lond)* 563: 529-539, 2005.

- 483 13. **Doolette DJ, Upton RN, and Zheng D.** Diffusion-limited tissue equilibration
484 and arteriovenous diffusion shunt describe skeletal muscle nitrous oxide
485 kinetics at high and low blood flows in sheep. *Acta Physiol Scand* 172: 167-
486 177, 2001.
- 487 14. **Duffner, G. J. and Snider, H. H.** Effects of exposing men to compressed air and
488 helium-oxygen mixtures for 12 hours at pressures of 2-2.6 atmospheres
489 (Research Report 1-59). Panama City (FL): Navy Experimental Diving Unit,
490 1958.
- 491 15. **Eckenhoff RG and Vann RD.** Air and nitrox saturation decompression: a report
492 of 4 schedules and 77 subjects. *Undersea Biomed Res* 12: 41-52, 1985.
- 493 16. **Eriksson E and Myrhage R.** Microvascular dimensions and blood flow in
494 skeletal muscle. *Acta Physiol Scand* 86: 211-222, 1972.
- 495 17. **Hales JRS.** Effect of exposure to hot environments on total and regional blood
496 flow in the brain and spinal cord of the sheep. *Pflügers Arch* 344: 327-337,
497 1973.
- 498 18. **Iversen PO, Standa M, and Nicolaysen G.** Marked regional heterogeneity in
499 blood flow within a single skeletal muscle at rest and during exercise
500 hyperaemia in the rabbit. *Acta Physiol Scand* 136: 17-28, 1989.
- 501 19. **Kety SS and Schmidt CF.** The determination of cerebral blood flow in man by
502 the use of nitrous oxide in low concentrations. *Am J Physiol* 143: 51-66, 1945.
- 503 20. **Kjellmer I, Lindberg I, Prerovsky I, and Tønnesen H.** The relation between
504 blood flow in an isolated muscle measured with the Xe¹³³ clearance and a
505 direct recording technique. *Acta Physiol Scand* 69: 69-78, 1967.
- 506 21. **Klein B, Kuschinsky W, Schrock H, and Vetterlein F.** Interdependency of
507 local capillary density, blood flow, and metabolism in rat brains. *Am J Physiol*
508 251: H1333-H1340, 1986.
- 509 22. **Lango T, Morland T, and Brubakk AO.** Diffusion coefficients and solubility
510 coefficients for gases in biological fluids: a review. *Undersea Hyperb Med* 23:
511 247-272, 1996.
- 512 23. **Novotny JA, Mayers DL, Parsons Y-FJ, Survanshi SS, Weathersby PK, and**
513 **Homer LD.** Xenon kinetics in muscle are not explained by a model of parallel
514 perfusion-limited compartments. *J Appl Physiol* 68: 876-890, 1990.
- 515 24. **Perl W, Rackow H, Salanitre E, Wolf GL, and Epstein RM.** Intertissue
516 diffusion effect for inert fat-soluble gases. *J Appl Physiol* 20: 621-627, 1965.
- 517 25. **Piiper J, Meyer M, and Scheid P.** Dual role of diffusion in tissue gas exchange:
518 blood-tissue equilibration and diffusion shunt. *Resp Physiol* 56: 131-144,
519 1984.

- 520 26. **Renkin EM.** Control of microcirculation and blood-tissue exchange. In:
521 *Handbook of Physiology. The Cardiovascular System. Microcirculation.*
522 Bethesda, MD: Am. Physiol. Soc., 1984, sect. 2, vol. 4, pt. 2, chapt. 14, p.
523 627-687.
- 524 27. **Schmidt-Nielsen K and Pennycuik P.** Capillary density in mammals in relation
525 to body size and oxygen consumption. *Am J Physiol* 200: 746-750, 1961.
- 526 28. **Sejrsen P and Tønnesen KH.** Inert gas diffusion method for measurement of
527 blood flow using saturation techniques. *Circ Res* 22: 679-693, 1968.
- 528 29. **Sejrsen P and Tønnesen KH.** Shunting by diffusion of inert gas in skeletal
529 muscle. *Acta Physiol Scand* 86: 82-91, 1972.
- 530 30. **Upton RN, Grant C, and Ludbrook GL.** An ultrasonic Doppler venous outflow
531 method for the continuous measurement of cerebral blood flow in conscious
532 sheep. *J Cereb Blood Flow Metab* 14: 680-688, 1994.
- 533 31. **Zheng D, Doolette DJ, and Upton RN.** In vivo manipulation and continuous
534 measurement of muscle blood flow with venous effluent sampling. *Clin Exp*
535 *Pharmacol Physiol* 27: 625-629, 2000.
536
537
- 538

539

540 **Table 1. Brain models parameter estimates and MSC**

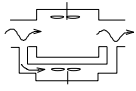
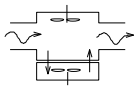
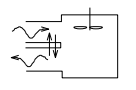
Model name	Model picture	Parameter name	Helium (He)	Nitrogen (N ₂)	He/N ₂
			Parameter value (S.D.) and MSC		
Perfusion-limited base		V ₁	60.3 (3.0)	51.9 (5.3)	54.2 (3.4)
		MSC	3.93	2.50	3.24
Two parallel perfusion-limited		V _{tot}	73.0 (3.9)	74.4 (9.8)	74.7 (4.9)
		F1	0.504 (0.081)	0.500 (0.108)	0.500(0.078)
		B1	0.874 (0.054)	0.932 (0.066)	0.917 (0.048)
		MSC	4.85	3.00	3.79
Perfusion-diffusion base		V ₁	34.8 (8.0)	24.9 (8.7)	28.3 (6.1)
		V ₂	38.2 (7.0)	58.1 (10.9)	54.4 (6.7)
		PS	18.3 (8.6)	13.1 (5.2)	13.9 (4.0)
		MSC	4.73	3.20	3.96
Perfusion-limited countercurrent diffusion		V ₁	82.3 (2.9)	93.2 (11.2)	78.3 (4.9)
		V _{ven}	10.1 (5.9)	18.9 (8.1)	7.97 (5.19)
		PSC	12.1 (2.3)	170 (50)	12.5 (4.1)
		MSC	4.99	3.14	3.73

541

542

543

Table 2. Hind limb models parameter estimates and MSC

Model name	Model picture	Parameter name	Helium (He)	Nitrogen (N ₂)	He/N ₂
			Parameter value (S.D.) and MSC		
Two parallel perfusion-limited		V _{tot}	1667 (189)	1150 (150)	1369 (128)
		F1	0.538 (0.020)	0.528 (0.025)	0.539 (0.016)
		B1	0.975 (0.003)	0.971 (0.005)	0.977 (0.003)
		MSC	2.72	2.42	4.04
Perfusion-diffusion base		V ₁	177 (12)	132 (13)	144 (9)
		V ₂	1472 (120)	1033 (112)	1156 (85)
		PS _R	82.4 (6.5)	82.0 (9.7)	82.1 (6.5)
		PS _L	11.2 (0.9)	10.9 (1.2)	11.0 (0.8)
MSC	3.14	2.60	4.30		
Perfusion-limited countercurrent diffusion		V ₁	1868 (145)	1336 (150)	1500 (117)
		V _{ven}	187 (16)	160 (21)	171 (16)
		PSC _R	47.5 (2.8)	50.3 (4.7)	48.9 (3.2)
		PSC _L	16.0 (1.0)	17.1 (1.7)	16.8 (1.2)
MSC	3.40	2.69	4.34		

544

Separate parameters for resting and low flow states denoted by subscripts R and L

545

546

547 Figure 1. Arterial and venous data from individual animals ($n = 5$) from the hind limb
548 in the resting flow state. The top panel shows the arterial helium concentrations (open
549 circles) along with the multi-exponential forcing function (solid line) fit to those data
550 and the femoral vein helium concentrations (filled circles) along with the mean data
551 (dashed line). Helium was administered during the interval zero to 20 minutes. The
552 bottom panel illustrates the nitrogen data. Arterial forcing functions were used as model
553 input and models were fit to the mean venous data. The variation in the individual
554 animal brain concentration data (not shown) was similar.

555 Figure 2. Single perfusion-limited compartments fit to the mean brain data. The fit
556 shown is for simultaneous fit to the nitrogen and helium data. Nitrogen was replaced
557 with helium in the breathing gas during the interval zero to 15 minutes. The left panels
558 illustrate the mean concentrations of helium (top panel) and nitrogen (bottom panel) in
559 arterial (open circles) and sagittal sinus (filled circles) blood samples taken during the
560 high cerebral blood flow state. The arterial input forcing functions are shown as dotted
561 lines. The model fit of the sagittal sinus blood concentrations are shown as solid lines.
562 The right panels illustrate the mean blood concentrations and model fit in the low
563 cerebral blood flow state.

564 Figure 3. Perfusion-diffusion compartment model fit to the mean brain data. The fit
565 shown is for simultaneous fit to the nitrogen and helium data. Nitrogen was replaced
566 with helium in the breathing gas during the interval zero to 15 minutes. Symbols and
567 lines are as in figure 2 except that the calculated nitrogen and helium concentrations in
568 the 'deep' compartment are shown as a dashed line (c2 calc).

569 Figure 4. Perfusion-limited countercurrent diffusion compartment model fit to the mean
570 hind limb data. The fit shown is for simultaneous fit to the nitrogen and helium data.
571 Nitrogen was replaced with helium in the breathing gas during the interval zero to 20
572 minutes. Symbols and lines are as in figure 2 except that the filled circles are the mean
573 helium or nitrogen concentrations in the femoral vein. Calculated nitrogen and helium
574 concentrations in the 'tissue' compartment are shown as a dashed line (c1 calc).

575

576

